# The LHCb Silicon Tracker

**Ch. Elsasser[c], B. Adeva[a], A. Gallas[a], E. Pérez Trigo[a], P. Rodríguez Pérez[a], A. Bay[b], F. Blanc[b], F. Dupertuis[b], G. Haefeli[b], I. Komarov[b], R. Märki[b], B. Muster[b], T. Nakada[b], O. Schneider[b], M. Tobin[b], M.T. Tran[b], J. Anderson[c], A. Bursche[c], N. Chiapolini[c], S. Saornil[c], S. Steiner[c], O. Steinkamp[c], U. Straumann[c], A. Vollhardt[c], M. Britsch[d], M. Schmelling[d], H. Voss[d], O. Okhrimenko[e], V. Pugatch[e]**

[a] *University of Santiago de Compostela, Santiago de Compostela, Spain.*
[b] *Ecole Polytechnique Fédérale de Lausanne (EPFL), Lausanne, Switzerland.*
[c] *Physik-Institut, Universität Zürich, Zürich, Switzerland.*
[d] *Max Planck Institut für Kernphysik (MPIK), Heidelberg, Germany.*
[e] *National Academy of Sciences, Institute for Nuclear Research, Kiev, Ukraine.*

ABSTRACT: The aim of the LHCb experiment is to study rare heavy quark decays and CP violation with the high rate of beauty and charmed hadrons produced in $pp$ collisions at the LHC. The detector is designed as a single-arm forward spectrometer with excellent tracking and particle identification performance. The Silicon Tracker is a key part of the tracking system to measure the particle trajectories to high precision. This paper reports the performance as well as the results of the radiation damage monitoring based on leakage currents and on charge collection efficiency scans during the data taking in the LHC Run I.

KEYWORDS: Silicon Tracker; LHCb; Silicon microstrip detector; Performance; Radiation Damage.

LHCb-PROC-2013-056
21/12/2013

## Contents



## 1. Introduction

The LHCb experiment [2] is designed for the study of heavy flavour physics in proton-proton collisions at the LHC. The primary goal of the experiment is to search for New Physics in rare decays of $b$ and $c$ hadrons and in precision measurements of CP violation.

The detector is set-up as a single-arm forward spectrometer covering a pseudorapidity range $\eta = -\log(\tan\theta/2)$ between 2 and 5, as $b\bar{b}$ and $c\bar{c}$ pairs are predominantly produced under small polar angles with respect to the LHC beams.

The Silicon Tracker (ST) is part of the tracking system and consists of two sub-detectors: the Tracker Turicensis (TT) placed upstream from the dipole magnet and the Inner Tracker (IT) forming the inner part of the tracking stations downstream from the dipole magnet. Both detectors use single-sided silicon micro-strip sensors. The TT has four planar detector layers ($0^\circ$, $+5^\circ$, $-5^\circ$ and $0^\circ$ tilted with respect to the field lines of the dipole magnet) made using $p^+$-on-n sensors with a strip pitch of 183 μm and a thickness of 500 μm. The sensors are bonded together into read-out sectors of either 1, 2, 3 or 4 sensors. This leads to read-out strips of up to 37 cm in length. In total there are about 144k read-out strips in the TT. The IT detector uses $p^+$-on-n type sensors with a strip pitch of 198 μm. They are grouped into twelve planar layers. In each layer the sensors in the region on both sides of the beam pipe are paired to form a read-out sector with a total strip length of 22 cm (long ladders). The sensors for this configuration have a thickness of 410 μm, while the read-out sectors below and above the beam pipe consist of single sensors which are 320 μm thick and have a read-out strip length of 11 cm (short ladders). The IT has around 130k read-out strips. Both detectors are operated with a sensor temperature of about $8^\circ$C.

The electronic read-out of the sensors is the same in both detectors: the Beetle front end

chip [3] amplifies, shapes and samples the output signal of the read-out strips which is then transmitted via up to 8 m long copper cables to service boxes close to the detector, but located outside of the acceptance. There the signal is digitized and transmitted via VCSEL[1] diodes and optical fibres to the counting house where the TELL1 boards [4] use FPGAs to perform pedestal and common mode noise subtraction as well as zero suppression.

## 2. Performance

At the end of LHC run I the fraction of working read-out channels in TT and IT was very high with 99.4 % and 98.4 %, respectively. The slightly smaller fraction in IT is due to the more difficult access to the detector during data taking periods. During the shutdown of LHC repair work has been done resulting in a recovery of a large fraction of bad read-out channels.

### 2.1 Time Alignment

The time alignment provides the synchronization of the trigger and control signals with the $pp$ collisions of LHC and takes into account differences in cable length and flight time of the particle among the different detector layers.

In ST it is performed by a scan over the delay between the sampling time of the Beetle chip with respect to the LHC clock. The signal amplitude is determined for each delay step of 6.2 ns as the most probable value (MPV) of the signal distribution. The position in time giving the highest signal amplitude is determined from a pulse fit to these data points. The procedure gives a time alignment better than 1 ns.

### 2.2 Signal-to-Noise Ratio

The signal-to-noise ratio ($S/N$) is measured in the ST using clusters from tracks with a reconstructed momentum larger than 5 GeV/c. The ratio is between 12 and 15 for TT, while for IT the range is 15 to 18. These values determined from data taken at the beginning of the data taking period in 2011 are close to expectations based on test beam measurements during the R&D phase [5]. Figure 1 shows the average $S/N$ in TT for 1-, 2-, 3- and 4-sensor read-out sectors as a function of the capacitance, and it displays the expected linear decrease of $S/N$ with increasing capacitance. In Fig. 2 the $S/N$ distribution for the long and short ladders in IT is shown. As the noise is dominated by the read-out electronics and the cabling, there is no significant change in $S/N$ due to detector ageing (cf. Sec. 3) expected.

### 2.3 Spatial Alignment

The alignment of the tracking stations in LHCb is based on a global minimisation of track residuals using a Kalman filter fit [6]. Further the alignment takes advantage of the possible mass constraints in $J/\psi \to \mu^+\mu^-$ and $D^0(\overline{D}^0) \to K^\pm\pi^\mp$ samples to constrain degrees of freedom which are weakly constrained by single tracks (e.g. global shearing or scaling of the detector) [7]. Fig. 3 shows the distributions of the minimized track residuals after the alignment procedure for TT and IT. The resulting hit resolutions in TT and IT including alignment effects are 61 μm and 54 μm respectively.

[1] Vertical-Cavity Surface-Emitting Laser

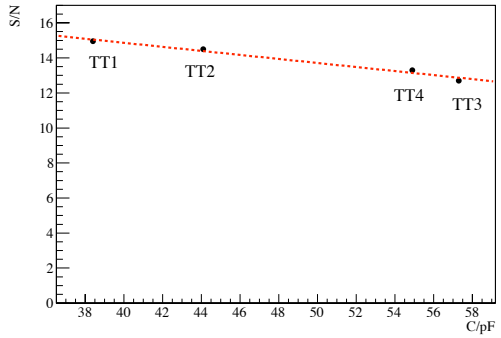


**Figure 1.** The average signal-to-noise ratio ($S/N$) vs the capacitance ($C$) of 1-, 2-, 3- and 4-sensor read-out sectors in TT. As expected $S/N$ decreases linearly as a function of $C$. The capacitance of the read-out sectors includes the cabling connection to the read-out electronics.

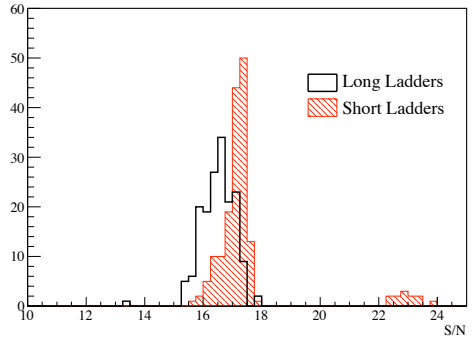


**Figure 2.** The signal-to-noise ratio ($S/N$) distribution for long ladders (black open histogram) and short ladders (red dashed histogram) in IT. The entries around 23 correspond to short ladders which were made out of 410 µm instead of 320 µm thick sensors.

In Fig. 4, the distributions of the average track residuals for each of the read-out sectors are shown for the 2012 data. From the RMS of these distributions the alignment precision is estimated to be 13.5 µm for TT and 15.0 µm for IT. These values are very good, especially when taking into account the fact that there are long distances between the tracking stations and that the tracking stations in LHCb are outside the magnetic field. Furthermore, LHCb is unable due to its forward geometry to use cosmics, which give a high statistics sample of tracks more uniformly distributed across the detector than tracks from $pp$ collisions.

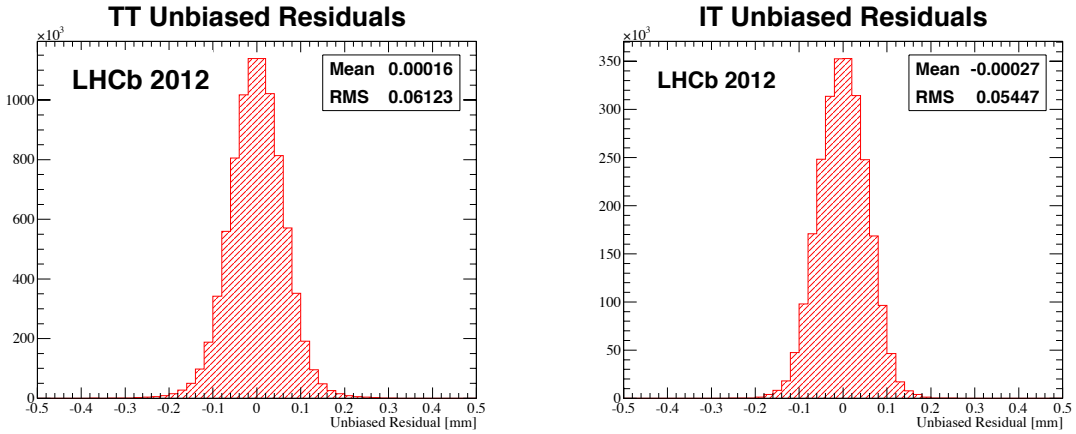


**Figure 3.** The track residual distributions after alignment for TT (left) and IT (right). The RMS of the distributions gives an estimate of the hit resolution including the residual alignment imperfection which is 61 µm for TT and 54 µm for IT.

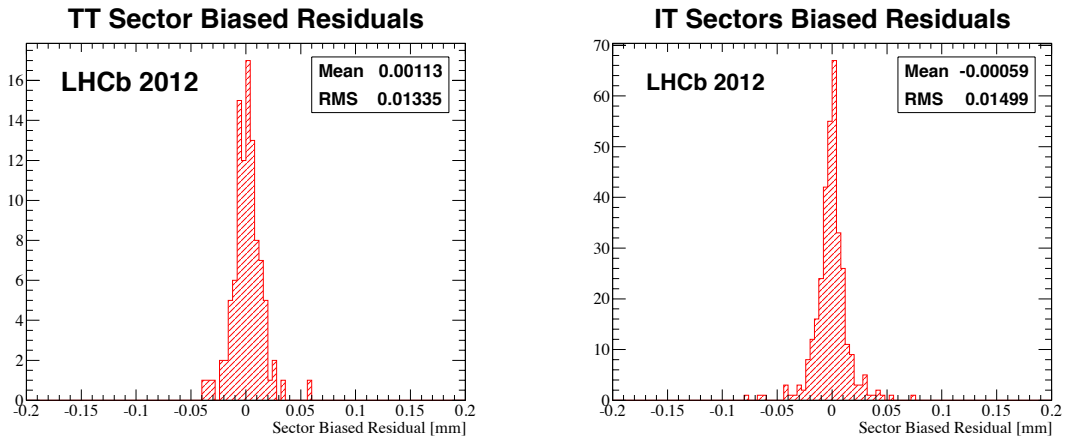


**Figure 4.** The distribution of the average track residual per read-out sector in TT (left) and IT (right) for 2012 data. The alignment precision of the two detectors is estimated from the RMS of these distributions. In the case of TT it is 13.5 µm, while for IT it is 15.0 µm.

### 2.4 Hit Efficiency

The hit efficiency in the ST is measured from data using isolated tracks with a momentum larger than 10 GeV/c. The track fit is repeated excluding the clusters in the sector under test. The hit efficiency is defined as the fraction of tracks that have a cluster in a search window around the track. The efficiency depends on the size of the search window and saturates at 99.3 % in IT and at 99.7 % in TT for search window sizes of 1.0 mm and 2.5 mm, respectively.

## 3. Radiation Damage

The monitoring of radiation damage effects is crucial to predict the long term performance of the detector. Two methods are applied to monitor radiation damage in the ST: the measurement of the leakage current and the estimation of the depletion voltage via dedicated Charge Collection Efficiency (CCE) scans.

### 3.1 Leakage Currents

The radiation leads to bulk damage in the silicon sensors which manifests itself by an increase of the leakage current $I_{\text{leak}}$. The leakage current is proportional to the total fluence

$$I_{\text{leak}} = \alpha \cdot \Phi_{1\text{ MeV-n,eq}} \cdot V \tag{3.1}$$

where $\Phi_{1\text{ MeV-n,eq}}$ is the 1 MeV-neutron equivalent fluence, $V$ the volume of the irradiated silicon and $\alpha$ is the damage factor for 1 MeV-neutrons taking into account annealing processes [9]. The effect of the temperature on $I_{\text{leak}}$ is given by

$$\frac{I_{\text{leak}}(T_1)}{I_{\text{leak}}(T_2)} = \left(\frac{T_1}{T_2}\right)^2 \cdot \exp\frac{E_g(T_1 - T_2)}{2k_B T_1 T_2}, \tag{3.2}$$

where $E_g$ is the band gap energy of silicon [10]. Figure 5 shows the peak currents per fill for the sensors closest to the beam pipe in two of the TT layers as a function of the delivered integrated luminosity. The currents are normalized to a temperature of 0° C using Eq. 3.2. The spread in $I_{\text{leak}}$ is caused by the difference in fluence across the detector. The prediction of the leakage currents based on a FLUKA simulation [8] is also displayed in Fig. 5 showing a good agreement with the measurement. The annealing taking place during the winter shutdown 2011/2012 is visible as a drop in $I_{\text{leak}}$ at about 1250 pb$^{-1}$.

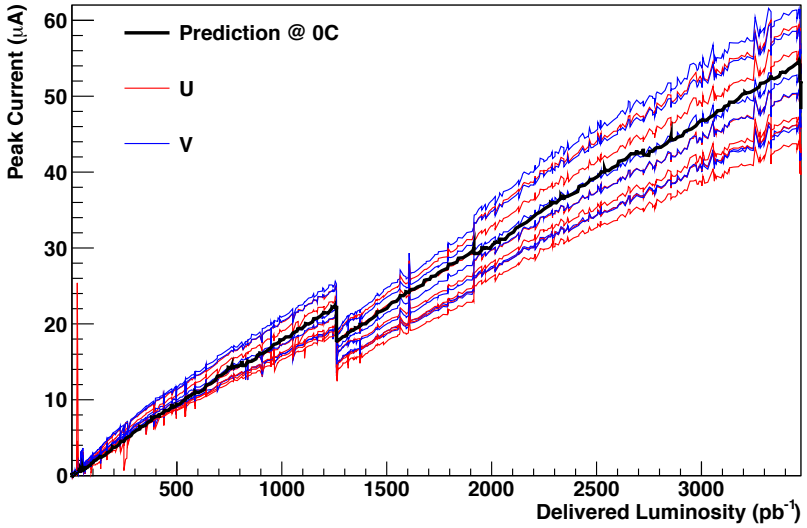


**Figure 5.** The peak leakage currents per fill for the sensors closest to the beam pipe in the second and third detection layers of TT as a function of the delivered integrated luminosity. The currents are normalized to a temperature of 0°C. The spread of the leakage currents is due to the difference in fluence across the sector. The prediction is based on the estimated fluence from a FLUKA simulation and takes also the annealing processes into account. The downward jump in the leakage current at an integrated luminosity of about 1250 pb$^{-1}$ corresponds to the annealing during the winter shutdown 2011/2012.

### 3.2 Charge Collection Efficiency Scans

Three to four times a year dedicated CCE scans take place. The goal of these scans is to measure the effective full-depletion voltage $V_{\text{depl}}$ of the silicon sensors. In these scans the bias voltage $V_{\text{bias}}$ is varied for one detection layer in TT and one in IT. Therefore tracks can be still reconstructed using the remaining layers. The extrapolation of the tracks to the scanned layers gives an estimation of the hit position. The summed signal amplitude of the three strips closest to this position is taken as signal amplitude associated to this track.

For each $V_{\text{bias}}$ setting the optimal sampling time is remeasured, following the procedure in Sec. 2.1, to correct for differences in the signal collection time in the silicon.
Figure 6 shows the distribution of the signal amplitudes in a read-out sector for a certain voltage and timing step. The noise distribution around zero is due to track extrapolations missing the track cluster as well as fake tracks created by combining hits from different particles. The MPV of the

signal amplitude distribution is extracted from a fit of a double Gaussian for the noise distribution and a convolution of the same double Gaussian with the sum of two Landau distributions. The Landau distribution with the larger yield is the signal contribution while the second Landau distribution smaller in yield (represented by the dotted line in the figure) takes photon conversion in the detector material into account. The maximum MPV of the signal height for a certain voltage step is extracted from a fit of the pulse shape described by a Half-Gaussian from the MPVs of the different sampling times.

Figure 7 shows the maximum MPVs as a function of the bias voltage.

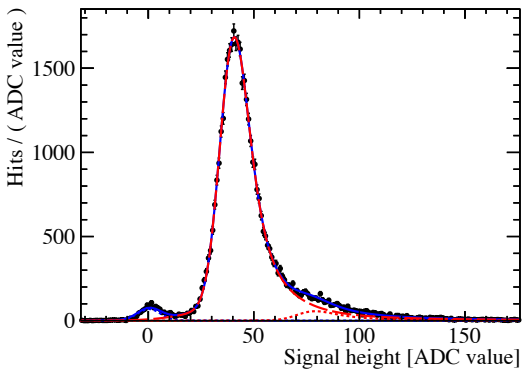


**Figure 6.** Distribution of the signal heights associated to the extrapolated tracks in the CCE scans for a bias voltage of 400 V. The distribution is described by a double Gaussian for the noise distribution around zero and a convolution of this double Gaussian with a Landau distribution (red dashed curve) for signal. A second Landau distribution convoluted with the double Gaussian (red dotted curve) takes photon conversion into account.

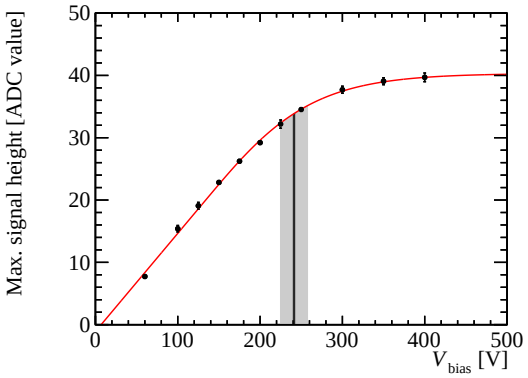


**Figure 7.** The measured maximal most probable value for signal heights as a function of the applied bias voltage (black dots) in a CCE scan from July 2011. The data is described by a sigmoid-like function (Eq. 3.3, red curve). The effective full-depletion voltage $V_{\mathrm{depl}}$ is extracted as the voltage where the function reaches 85 % of its maximum. This voltage value is displayed by the black vertical line. The grey band shows the uncertainty on $V_{\mathrm{depl}}$.

A sigmoid-like function of the form

$$f(V_{\mathrm{bias}}) = \begin{cases} \frac{A_0}{1+\exp[r(V_{\mathrm{bias}}-V_0)]} & \text{if } V_{\mathrm{bias}} \geq V_0 \\ \frac{A_0}{2}[1+\frac{r}{2}(V_{\mathrm{bias}}-V_0)] & \text{if } V_{\mathrm{bias}} < V_0 \end{cases} \tag{3.3}$$

is used to describe the data points. The effective full-depletion voltage is defined as the bias voltage where the function reaches 85 % of its maximum value. This value of 85 % has been determined by comparing the results on non-irradiated sensors in the earliest CCE scan with $V_{\mathrm{depl}}$ determined from measured $1/C^2$-curves during the detector production.

The measured full-depletion voltage values from all TT read-out sectors in all CCE scans are shown in Fig. 8 as a function of the corresponding 1 MeV-neutron equivalent flux estimated from FLUKA simulations. As expected there is a decrease in $V_{\mathrm{depl}}$ in the highest irradiated region of TT. The black line in the figure shows the estimated change in $V_{\mathrm{depl}}$ based on the stable damage part of the Hamburg model [11] and is in good agreement with the measurements. The evolution of the

effective full-depletion voltage as a function of time using clusters associated with tracks in a region closer than 45 mm to the beam axis is shown in Fig. 9. The plot shows also the prediction from the full Hamburg model based on the actual running conditions. There is a very good agreement between prediction and measurement.

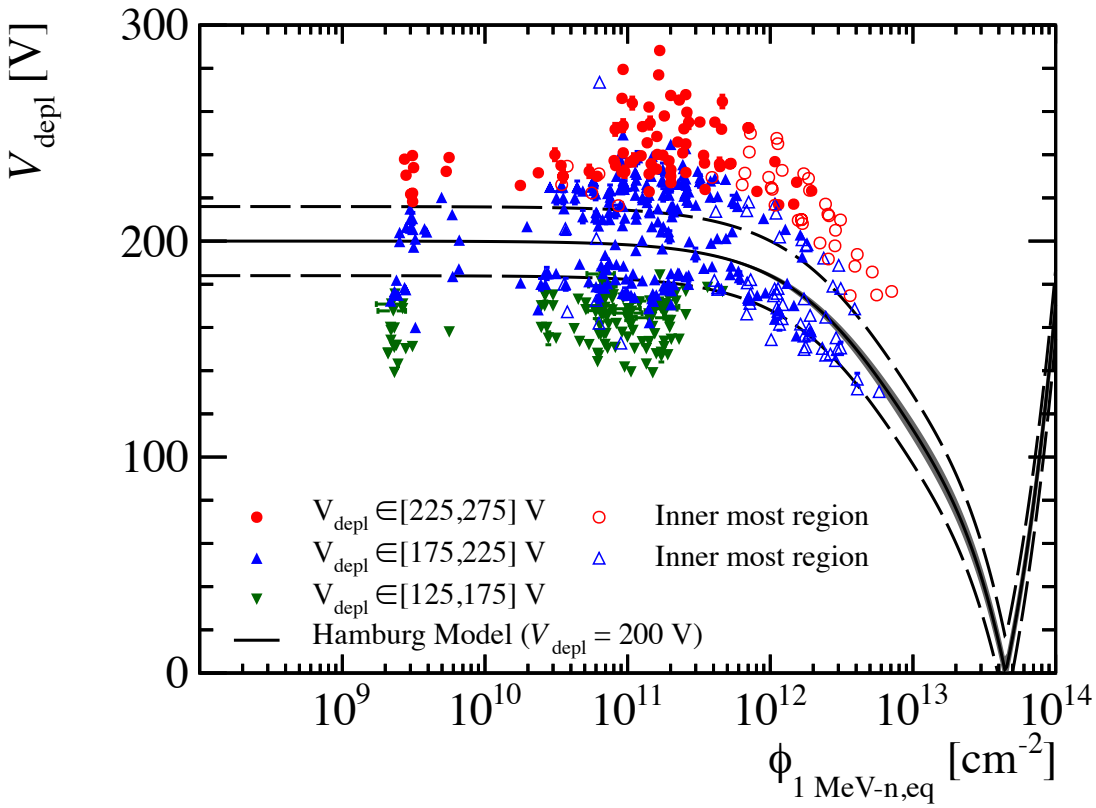


**Figure 8.** The effective depletion voltage measured for different read-out sectors of TT and in different CCE scans as a function of the estimated 1 MeV-neutron equivalent flux. The black line shows the predicted evolution of the depletion voltage starting at 200 V based on the stable damage part of the Hamburg model. The narrow shaded band around the line displays the uncertainty on the prediction propagated from the uncertainties on the model parameters. The black dashed lines show the average total uncertainty on the measured depletion voltage values.

## 4. Summary

The LHCb Silicon Tracker has shown an excellent performance during LHC Run I between 2010 and 2012. The observed signal-to-noise ratios are for both sub-detectors (TT: 12-15, IT: 15-18) close to the expectation from test beam results during the R&D phase. The spatial alignment, which is in LHCb done based on collision data, has a precision better than 15 µm. The precision of the time alignment is better than 1 ns and the hit efficiency is for both detectors well above 99 %.

The monitoring of the radiation damage done by measuring leakage currents and the effective full-depletion voltage shows very good agreement with expectations based on the running condi-

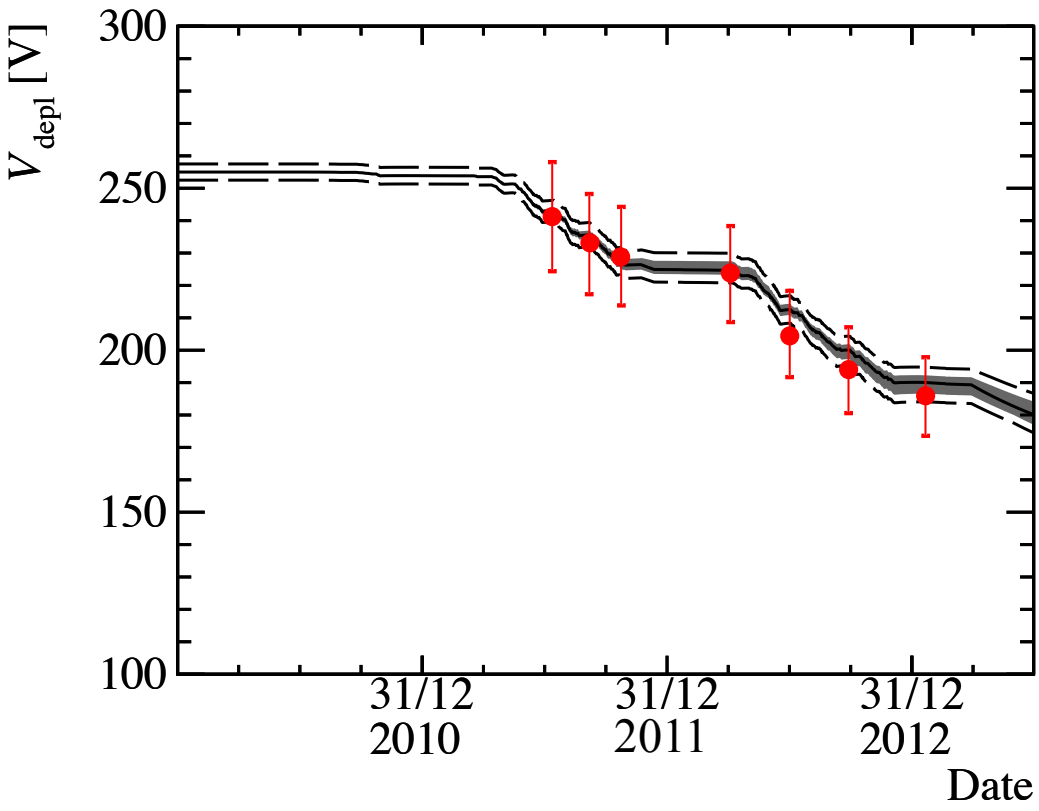


**Figure 9.** The measured effective depletion voltage for the region closer than 45 mm to the beam axis in the TT sensor closest to the beam pipe (red dots) as a function of time. The error bars show the combined statistical and systematic uncertainties. The black line shows the predicted change in the depletion voltage based on the full Hamburg model and the actual running conditions of LHCb (delivered luminosity, sensor temperature). The band around the line shows the uncertainty on the prediction while the black dashed lines show the additional uncertainty from the initial measurement of the depletion voltage after production.

tions. These measurements show that both sub-detectors will be able to cope with the radiation in LHCb up to the planned upgrade of the detector during long shutdown 2 (LS2).

During the long shutdown 1 (LS1) minor maintenance work is performed on the Silicon Tracker such that it will be ready to continue operation with an excellent performance after the restart of the LHC.

## References

[1] Ch. Elsasser et al., *The LHCb Silicon Tracker* (2013), LHCb-PROC-2013-056.

[2] A.A. Alves et al., *The LHCb Detector at the LHC*, JINST 3 (2008) S08005.

[3] M. Agari et al., *Beetle: A radiation hard read-out chip for the LHCb experiment*, *Nucl. Instrum. and Meth.* **A518** (2004) 468-469.

[4] G. Haefeli et al., *The LHCb DAQ interface board TELL1*, *Nucl. Instrum. and Meth.* **A560** (2006) 494-502.

[5] M. Agari et al., *Test beam results of multi-geometry prototype sensors for the LHCb Inner Tracker* (2002), LHCb-2002-058.

[6] W. Hulsbergen, *The global covariance matrix of tracks fitted with a Kalman filter and an application in detector alignment*, *Nucl. Inst. Meth.* **A600** (2009) 471, [physics.ins-det/0810.2241v2].

[7] J. Amoraal et al., *Application of vertex and mass constraints in track-based alignment*, *Nucl. Inst. Meth.*, **A712** (2013) 48-55, [physics.ins-det/1207.4756v2].

[8] A. Ferrari et al. *FLUKA: a multi-particle transport code* (2005), CERN-2005-10, INFN/TC_05/11, SLAC-R-773.

[9] M. Moll et al., *Leakage current of hadron irradiated silicon detectors - material dependence*, *Nucl. Instrum. and Meth.* **A426** (1999) 87-93.

[10] S.M. Sze, *Physics of Semiconductor Devices*, Wiley-Interscience, New York 1985.

[11] M. Moll, *Radiation Damage in Silicon Particle Detectors* (1999), DESY- THESIS-1999-040.